High-resolution architecture of the outer membrane of the Gram-negative bacteria Roseobacter denitrificans.

Szymon Jaroslawski, Katia Duquesne, James N. Sturgis, Simon Scheuring

▶ **To cite this version:**

Szymon Jaroslawski, Katia Duquesne, James N. Sturgis, Simon Scheuring. High-resolution architecture of the outer membrane of the Gram-negative bacteria Roseobacter denitrificans.. Molecular Microbiology, 2009, 74 (5), pp.1211-1222 ⟨10.1111/j.1365-2958.2009.06926.x⟩. ⟨inria-00436539⟩

HAL Id: inria-00436539

https://inria.hal.science/inria-00436539v1

Submitted on 27 Nov 2009

HAL is a multi-disciplinary open access archive for the deposit and dissemination of scientific research documents, whether they are published or not. The documents may come from teaching and research institutions in France or abroad, or from public or private research centers.

L'archive ouverte pluridisciplinaire **HAL**, est destinée au dépôt et à la diffusion de documents scientifiques de niveau recherche, publiés ou non, émanant des établissements d'enseignement et de recherche français ou étrangers, des laboratoires publics ou privés.

HAL Authorization

THIS IS A PRE-PRINT, NON PEER-REVIED VERSION OF THE ARTICLE

High-resolution architecture of the outer membrane of the Gram-negative bacteria *Roseobacter denitrificans*

Szymon Jarosławski[1], Katia Duquesne[2], James N Sturgis[2] & Simon Scheuring[1]*

[1]Institut Curie, Équipe INSERM Avenir, UMR168-CNRS, 26 Rue d'Ulm, 75248 Paris Cedex 05, France.

[2]LISM, CNRS - Aix Marseille University, 31 Chemin Joseph Aiguier, 13402 Marseille cedex 20, France.

* Correspondence to S. Scheuring

Tel: ++33-1-56246781

Fax: ++33-1-40510636

Email: simon.scheuring@curie.fr

Keywords:

AFM / bacterial porin / membrane structure / native protein assembly / peptidoglycan

Abbreviations:

2D: two-dimensional / AFM: atomic force microscopy / *E*: Escherichia / LPS: lipopolysacharide /OM: outer membrane / SD: standard deviation / SDS-PAGE: sodium dodecyl sulfate polyacrylamide gel electrophoresis / *R*: Roseobacter / *Rb*: Rhodobacter / wt: weight

Manuscript statistics:

Title characters: 95 / Running title characters: 28 / Abstract words : 169 / Total character count : 39472

Summary

The outer membrane of Gram-negative bacteria protects the cell against bactericidal substances. Passage of nutrients and waste is assured by outer membrane porins, beta-barrel transmembrane channels. While atomic structures of several porins have been solved, so far little is known on the supramolecular structure of the outer membrane. Here we present the first high-resolution view of a bacterial outer membrane gently purified maintaining remnants of petidoglycan on the perisplasmic surface. AFM images of outer membrane fragments of the size of ~50% of the bacterial envelope revealed that outer membrane porins are by far more densely packed than previously assumed. Indeed the outer membrane is a molecular sieve rather than a membrane. Porins cover ~70% of the membrane surface and form locally regular lattices. The potential role of exposed aromatic residues in the formation of the supramolecular assembly is discussed. Finally, we present the first structural data for the outer membrane porin from a marine Gram-negative bacteria *Roseobacter denitrificans*, and we perform a sequence alignment with porins of known structure.

Introduction

Gram-negative bacteria protect themselves against the environment with an outer membrane (OM), which acts as a permeability barrier and creates the periplasmic space, an additional aqueous compartment. The OM has to allow both the influx of nutrient molecules and secretion of waste products and various factors for interaction with the environment (Nikaido, 2003). The barrier functions of the OM are assured by an asymmetric lipid bilayer with an inner leaflet composed of phospholipids and an outer leaflet of lipopolysaccharides (LPS) (Rosenbusch, 1974). The transport function is assured by a collection of transmembrane proteins, which form

selective, gated, and sometimes energized, channels across the membrane. The simplest and most abundant of these are the trimeric-porins, such as OmpF of *Escherichia (E.) coli*, which are the major protein components of the OM, and allow permeation of hydrophilic molecules with a mass of less than about 600 Da (Cowan et al., 1992). X-ray structures are available for several of these major porins (which are typically trimeric): from *E. coli* OmpF (Cowan et al., 1992), OmpC and PhoE (Schirmer, 1998), as well as for two porins from the α-3-subgroup of freshwater proteobacteria, *Rhodobacter (Rb.) blasticus* (Kreusch & Schulz, 1994) and *Rhodobacter (Rb.) capsulatus* 37b4 (Weiss & Schulz, 1992). Beyond the trimeric porins many other proteins are found in the outer-membrane for example in *E. coli* these include: specific transporters such as BtuB or FecA (Locher et al., 2002), which act as TonB energized transporters of vitamin B12 and iron citrate respectively (Shultis et al., 2006), monomeric porins such as OmpA (Pautsch & Schulz, 2000) or OmpX (Vogt & Schulz, 1999), more complex secretion machines such as TolC or Wza (Nikaido, 2003). However, though the structures of many individual outer membrane proteins are solved, and it has been estimated that a single *E. coli* cell possessed 10^5 molecules of its major porin OmpF (Rosenbusch, 1974), little is known about the supramolecular organization of the bacterial outer membrane.

The atomic force microscope (AFM) (Binnig et al., 1986), since its invention over 20 years ago, has become a powerful tool for studying biological membranes. Its most unique application is high-resolution imaging that can be performed in aqueous environment at ambient temperature and pressure with virtually no need for invasive fixation or staining procedures (Karrasch et al., 1994). High-resolution AFM topographs of membrane protein 2D-crystals (Schabert et al., 1995), densely packed reconstitutions (Seelert et al., 2000), and the supramolecular protein assembly in membranes of purple bacteria (Scheuring et al., 2005) have been reported. Equally, the morphology and interactions of the outer cell wall surface of bacteria have been studied on life cells (Dufrêne, 2008).

AFM has been used to image the outer membrane porin OmpF from *E. coli* after reconstitution into 2D-crystals (Schabert et al., 1995), however the native outer membrane of a Gram-negative bacteria has not been observed to date by AFM or any other technique.

In this article we examine the OM of a marine aerobic anoxygenic prokaryote *Roseobacter (R.) denitrificans.* This species has not been very extensively studied biochemically despite its widespread occurrence amongst marine picoplankton and its fully sequenced genome (Swingley et al., 2007). The major porin of this bacterium has 44% and 41% sequence similarity with *Rb. blasticus* and *Rb. capsulatus* porins respectively, and likewise has been proposed to form homo-trimers (Neumann et al., 1997). We present the first high-resolution information on the native supramolecular assembly of porins in native outer bacterial membranes. Furthermore, we report the first structural data of the major *R. denitrificans* porin and analyze how it reflects its amino acid sequence.

Results and Discussion

Composition of Roseobacter denitrificans outer membrane

R. denitrificans is a small Gram-negative α-proteobacteria typically about 1 to 1.5 μm long and slightly less than 1 μm in diameter (**Fig. 1A**). Cells were broken and the outer membranes prepared as described in the methods section, to give large membrane vesicles and fragments up to 1-2μm in diameter (**Fig. 1B**). The large size of the vesicles, which represent about 50% of the surface (~3 μm^2) of a bacterium, suggests that there is unlikely to be much difference between the architecture analyzed and the overall composition of the OM *in situ*.

To investigate the composition of the purified OM of *R. denitrificans* we have compared the protein composition (**Fig. 1C**), and phospholipid / sugar / protein ratio to that of *E. coli* OM

prepared by the same protocol. The SDS-PAGE analysis shows that the membrane has a less

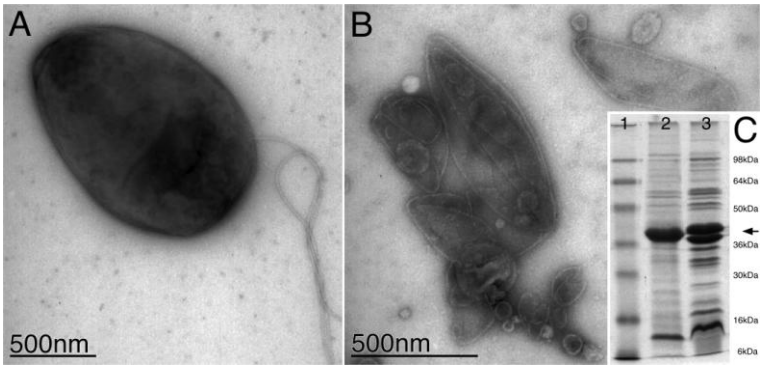

Fig. 1) Characterization of the *R. denitrificans* OM. **(A)** Electron micrograph of a *R. denitrificans* cell. **(B)** Electron micrograph of OM fragments. The sample preparation results in membranes that are a significant percentage of the total OM of a cell. **(C)** SDS-PAGE analysis: lane 1, marker; lane 2, *R. denitrificans* OM; lane 3, *E. coli* OM.

varied composition than that of *E. coli*. The major porin band at ~40 kDa represents for *R. denitrificans* about 90 % of the protein in the membrane. In *E. coli* about 80 % of OM protein constitute the major band, which corresponds to the trimeric porins OmpF and OmpC (**Fig. 1C**). Composition analysis of the membrane sample showed a phospholipid / sugars / protein ratio of 0.17 / 0.61 / 1 (wt / wt / wt) for *R. denitrificans*. The same analysis of *E. coli* OM yielded 0.14 / 0.35 / 1, probably indicating a larger LPS than in *E. coli*, more sugars per LPS molecule and thus per surface area, or possibly less complete digestion of the peptidoglycan. Overall the OM in *R. denitrificans* is slightly less complex but comparable to that of *E. coli*.

An ill-defined peptidoglycan layer on the periplasmic surface

The isolation procedure allowed us to observe diverse membrane specimens and virtually no protein-free phospholipid sheets. The large OM vesicles flattened and eventually opened on the mica AFM support. As a result, we observed single layers (**Fig. 2A**) or stacks of the OM fragments. The stacks were composed of two and rarely four layers adsorbed on the mica (**Fig. 3A**).

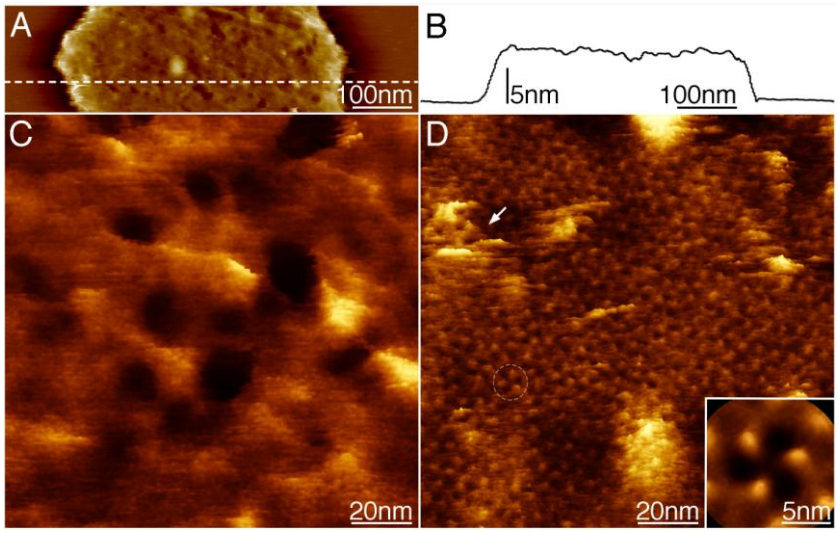

Fig. 2) Periplasmic OM surface and removal of the peptidoglycan layer with the AFM tip. (A) Overview topograph of a single layered OM patch. **(B)** Section analysis along the dashed line in (A). **(C)** Topograph of the periplasmic OM surface covered by peptidoglycan. **(D)** Repetitive scanning uncovers the underlying periplasmic surface of the outer membrane porins. Encircled is a single porin trimer. The arrow indicates remnant peptidoglycan. The inset shows a three-fold symmetrized average *(n=45).*

A portion of OMs did not form vesicles or double layers but rather large flat single layered fragments. Initially, no protein was visible in these membranes (**Fig. 2A**). We suspected that this was due to peptidoglycan adhering to the periplasmic surface that had not been completely removed by the lysozyme treatment. The thickness of these membranes was highly variable around 7 nm (**Fig. 2B**). The morphology of the peptidoglycan layer is heterogeneous (**Fig. 2C**).

Repetitive scanning of the ill-defined peptidoglycan layer (**Fig. 2C**) with slightly increased loading force allowed removal of the film and obtain images of the single-layered membranes (**Fig. 2D**). An average (**Fig. 2D**, inset) calculated from the particles found in these topographs (**Fig. 2D**, circle) compared well with the periplasmic surface of the X-ray structures of the homologue OM porins from *Rb. capsulatus* (PDB: 2POR) and *Rb. blasticus* (PDB: 1PRN). This assignment is also in agreement with the native morphology of the OM, where peptidoglycan layers the periplasm (Rosenbusch, 1974).

Nanodissection of membrane stacks: the periplasmic and the extracellular OM surfaces

More abundant in the sample preparation were OM stacks (**Fig. 3A**). Their thickness was multiples of ~5.3 nm (**Fig. 3B**). The most prevalent specimen were sandwich-like double bilayer stacks in which the periplasmic surface is hidden and the extracellular surface is exposed to the AFM tip (**Fig. 3C**). This orientation resembles the native orientation of the outer membrane, but is inversed with respect to the often also stacked reconstitutions of the OmpF in 2D-crystals (Hoenger *et al.*, 1993, Schabert & Engel, 1994). On the extracellular surface, each porin trimer displayed three protrusions of ~ 5Å height beyond the surface accessible by the AFM tip. As reported in the previous AFM study of OmpF porin reconstituted in 2D-crystals, these protrusions correspond to the long loops connecting β-strands of transmembrane barrels (Schabert et al., 1995).

We observed that the extracellular surface of the porin existed in two distinct conformations (**Fig. 3C**, circled). These two conformations of the extracellular domains (**Fig. 3C, D**) were found reproducibly: less frequent, one with separated protrusions (**Fig. 3D**, top) and another with protrusions contracted at the three-fold axis (**Fig. 3D**, bottom). Their occurrence was correlated with their position within the membrane: trimers, which were positioned in the center of a membrane displayed the „relaxed“ conformation (**Fig. 3D**, top), while trimers at the membrane edges displayed the „contracted“ conformation (**Fig. 3D**, bottom). The “relaxed” conformation of external loops compares to the X-ray structures by the OM porin from *Rb. blasticus* and OmpF from *E. coli*, as further elaborated along with the sequence analysis (see figure 7).

Distinct conformations on the extracellular surface have previously been observed for the *E. coli* OmpF (Schabert et al., 1995). OmpF in the “relaxed” conformation were proposed to from salt bridges with neighboring molecules in densely packed 2D-crystals (Schabert et al., 1995). Alternatively, it has been proposed that the “contracted” conformation results from a shift of the extracellular protrusions of the porin towards its three-fold axis and leads to contraction of the central cavity. In that study on OmpF 2D-crystals it was shown that the conformational change of the extracellular protrusions could be triggered by ions trapped underneath membrane layers that generated a Nernst potential (Müller & Engel, 1999).

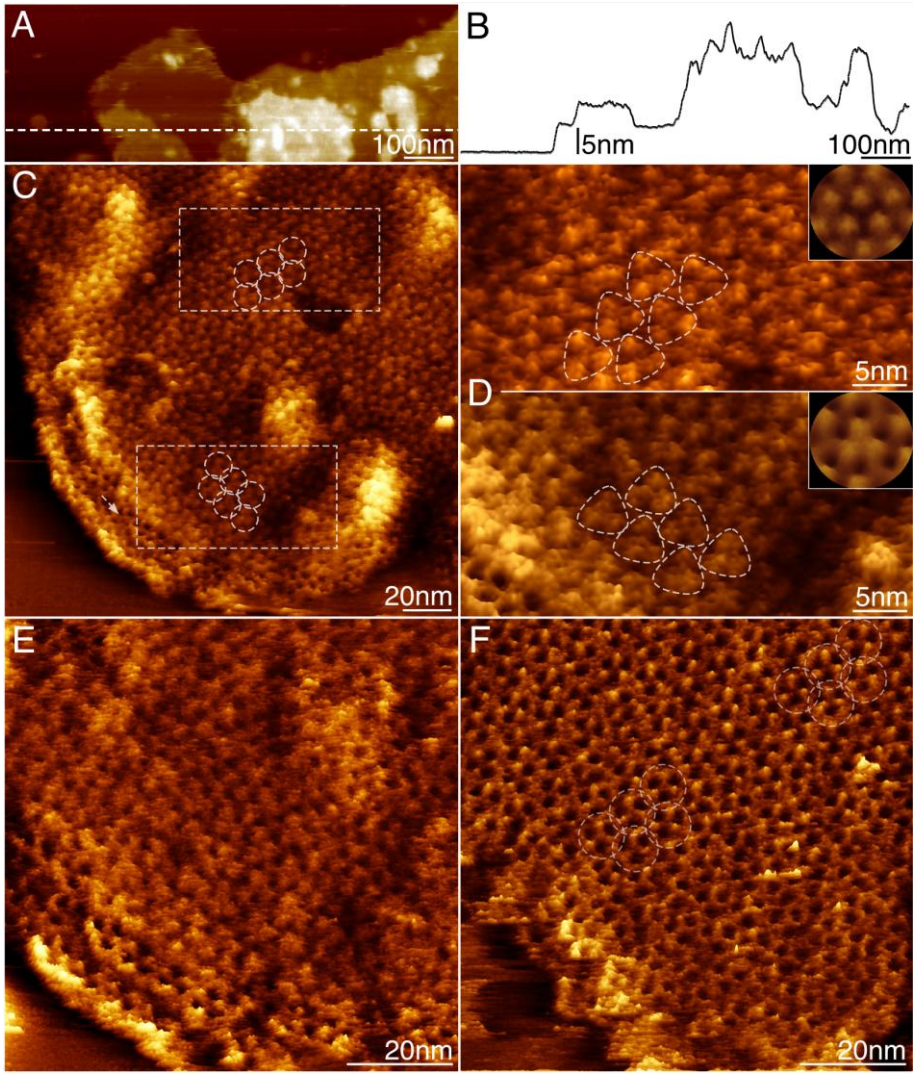

Fig. 3) Nanodissection of membrane stacks allowed visualization of both, the extracellular and the periplasmic OM surfaces. (A) Topograph of a large OM fragment containing single, double and four-layer sheets. **(B)** Section analysis along the dashed line in (A). **(C)** Topograph of the top layer exposing the extracellular surface to the AFM tip. The arrow marks a border strip, which exposes the underlying layer showing the periplasmic surface. Encircled are trimers representing two different conformations of the extracellular domains. **(D) T**he two conformations of the extracellular protrusions correlate with their location within the membrane. The „relaxed" conformation (top) was found inside the membrane patch (dashed outlines). The 3-fold symmetrized average (*n=30*) discloses a well-preserved, central indentation. The „contracted" conformation (bottom) displayed by porin located close to the membrane's border (dashed outlines). The three-fold symmetrized average (*n=20*) reveals the absence of central depression. **(E** and **F)** Nanodissection of the top layer exposing the extracellular surface (E) uncovers the lower layer exposing the periplasmic surface (F). Regions with porins in a hexagonal packing order are abundant (dashed outlines in F).

We hypothesize that the conformational variability that we observed, which coincided with the molecules location within the membrane (**Fig. 3C, D**), agrees with the effect described by

Müller. The ion gradient emerging from the divalent ions used for membrane adsorption equilibrates rapidly at the membrane boarder, while ions are firmly trapped underneath the central region of the membrane. Functionally, the existence of different conformational states in porins from *E. coli* K12 has also been reported by conductance measurements (Todt *et al.*, 1992, Buehler *et al.*, 1991).

Using the AFM tip for imaging and as a nanodissector (Scheuring *et al.*, 2004, Scheuring *et al.*, 2003), it was possible to first image at high resolution the extracellular surface (**Fig. 3E**), remove the top layer by means of the tip, and then, returning to imaging mode, scan the periplasmic surface of the layer adsorbed on the mica (**Fig. 3F**). The fact that the top layer was sensitive to scanning forces slightly higher than 100pN is in agreement with observations on OmpF 2D-crystals (Schabert et al., 1995).

High-resolution analysis of the periplasmic OM surface

In contrast to the extracellular surface of the OM, the periplasmic side could be scanned on single-layered flat membranes, which were adsorbed directly on the mica support (**Fig. 3F, 4A**). This allowed high-resolution scanning revealing sub-molecular details (**Fig. 4B**). Unlike the previous AFM studies of *E. coli* OmpF reconstituted in 2D-crystals (Müller & Engel, 1999, Schabert et al., 1995), our topographs represent molecules in their native membrane. Viewed from the periplasmic surface, the porins exhibit oval-shaped cavities separated by walls crowned by three major protrusions. Furthermore, fine topographic features are detectable at the three-fold axis and at the pore brims (**Fig. 4B**). The visibility of some structural features was enhanced by averaging (Fechner et al., 2009), resulting in an average (**Fig. 4C**) that compared with an astonishing resemblance the molecular surface of the X-ray structure of the homologue *Rb. capsulatus* porin (Weiss & Schulz, 1992) on the periplasmic surface (**Fig. 4D**). The highest

periplasmic protrusion revealed a slight bi-lobe structure that originates from the turns β2-β3 (arrow 1) and β14-β15 (arrow 1') from two barrels within the trimer. Most astonishingly, the AFM resolved a faint protrusion close to the trimer center (arrow 2): this is the N-terminal end of β-strand 1, and corresponds most probably to a single amino acid, Asp1 (Glu1 in *Rb. capsulatus*).

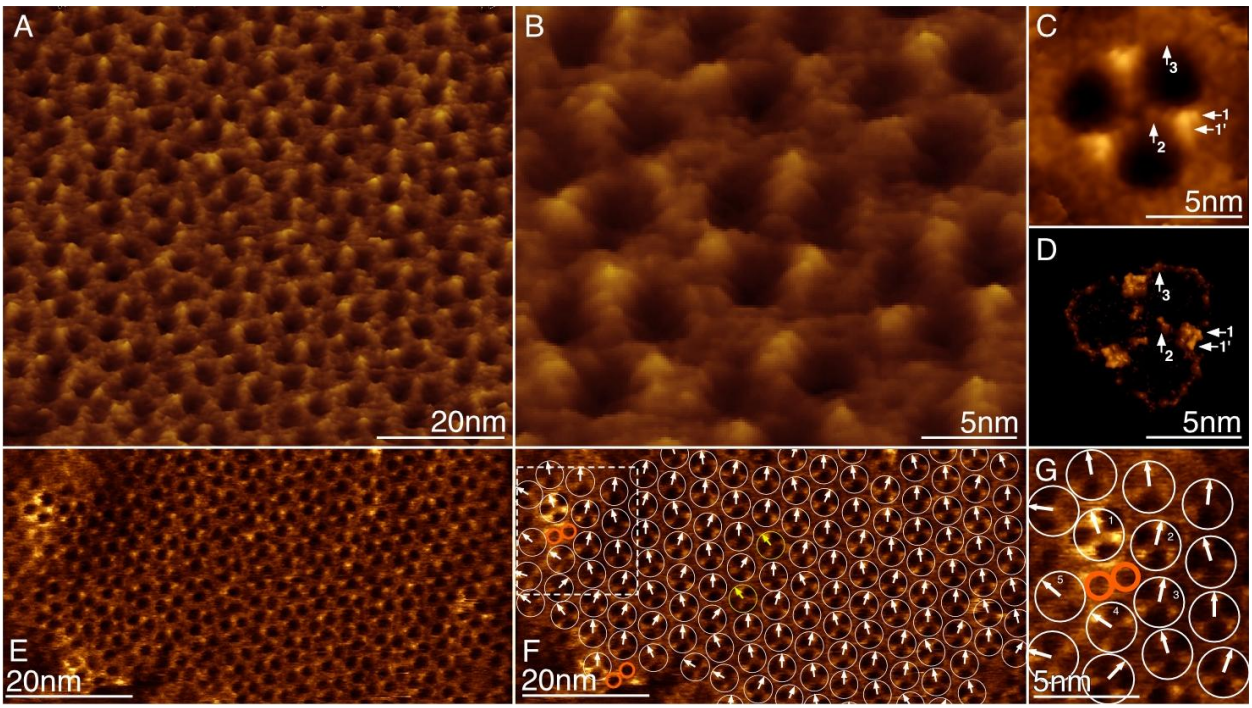

Fig. 4) High-resolution analysis of the periplasmic surface of the *R. denitrificans* OM and position and rotation order of trimeric porins and non-trimeric porins. (**A**) Membrane region densely packed with porin trimers. (**B**) At high resolution substructure is visible on individual trimers. (**C**) Average (*n=18*) reveals major peripheral protrusions (turn β2-β3, arrow 1 and turn β14-β15, arrow 1'), fine protrusions (N-terminal Asp1) close to the trimer axis, and a peripheral protrusion (turn β12-β13, arrow 3). (**D**) Structure of the periplasmic side of the *Rb. capsulatus* porin (PDB: 1PRN) shows high similarity to the average. **(E)** High-resolution AFM topograph. **(F)** Circle and arrow outlines of the position and rotation of trimeric porins. Exclusion of all pores attributable to trimers, identified non-trimeric porins (orange outline). **(G)** Close-up view on the non-trimer porins (orange outlines). The neighboring pores constitute five porin trimers (numbered 1 to 5).

Finally, the turn β12-β13 is visible (arrow 3), consisting of a proline and a valine. Such high resolution achieved in the AFM topographs suggests a high stability of short β-turns. Similar results were obtained on OmpF 2D-crystals (Müller et al., 2000), while the resolution on loops of

α-helical membrane proteins is slightly inferior (Scheuring *et al.*, 1999, Buzhynskyy *et al.*, 2007).

The major porin in the native membrane of *R. denitrificans* is ordered in the most densely packed regions (**Fig. 4E**). In these, the unit cell a = b = 81 Å ± 2.5 Å, γ = 60º (*n* = 24) occupies an area of ~6000 Å^2. From the X-ray structure of the homologue trimeric porin from *Rb. capsulatus* we calculated, that the trimer occupies an in-membrane-plane area of ~4500 Å^2. This means that porins cover ~ 75% of the membrane surface. In less ordered regions the protein density is still high, between ~60% and ~75%. Because the lipids are restricted to the intermolecular spaces between porins in the dense packing, we estimate the presence of about 30 phospholipids in the periplasmic leaflet and about 10 lipopolysaccharides in the external membrane leaflet per unit cell and porin trimer.

From visual inspection, it is impossible to evaluate the lateral and rotational order of the molecules, nor to tell if there are other than trimeric porins within the membrane (**Fig. 4E**). For this we used a cross-correlation search approach (Fechner et al., 2009) for trimeric porins, that results in a trimer porin coordinates and orientation list. This allowed us on the one hand to evaluate the positional and orientation regularity of the trimers in the densely packed regions, and on the other hand to identify pores that do not participate in trimer formation (**Fig. 4F**). From this analysis, we learned, first that the positional precision of the molecule location has a standard deviation (SD) of 5.4 Å (individual molecular position is significantly les well preserved that the lattice analysis, SD = 2.5 Å, described above). Second, the molecules are rotationally not well aligned with a SD of 10º. The alignment of molecules towards the membrane edge deviated strongly from the alignment of the majority of trimers, but also some molecules inside the ordered area are ill aligned (**Fig. 4F**, yellow arrows). Third, some pores are not participating in trimers (**Fig. 4F**, orange outline). Indeed, cross-correlation searches assigned unambiguously the five porin trimers surrounding two pores left odd (**Fig. 4G**). We assign these

pores to the homologous porin to *E. coli* Fhua that was shown to be dimeric in the membrane (Lambert et al., 1999), or two of any of the monomeric porins (homologous to OmpX, OmpW, OmpA, OmpG, etc). As shown by our biochemical analysis, in *R. denitrificans* the major trimeric porin comprises an even higher percentage of the total OM protein content than the trimeric porins in *E. coli* (see figure 1C).

Genome analyses suggested that α-proteobacteria possessed exceptionally few genes coding for OM β-barrel proteins when compared to other proteobacterial classes (Gatsos et al., 2008). While most other proteobacteria proteomes posses more than 100 β-barrel proteins, a detection of β-barrel proteins in the entire *R. denitrificans* proteome, which we performed with the BOMP platform, retrieved only 25 proteins, of which only eight were supported by matches with the BLAST search (Berven et al., 2004). This could explain the apparent protein homogeneity of the *R. denitrificans* OM, and the very few non-trimer porins found.

Even more astonishing is our finding that the OM of the marine α-proteobacterium *R. denitrificans* is a continuous "molecular sieve", which does not comply with the amended fluid mosaic model proposed for membranes (Singer & Nicolson, 1972, Engelman, 2005). Because of high structural homology between the studied porin and other bacterial porins we believe that this organization is common in all Gram-negative species where the outer membrane plays essentially the same role. Therefore, our discovery should change the way scientists interpret and design future studies of OM proteins. Particularly, all computational simulation studies of OM proteins to date have ignored inter-molecular interactions that may arise between individual proteins in dense packing (Khalid *et al.*, 2006, Domene *et al.*, 2003, Bond & Sansom, 2004). Recently, molecular dynamics studies of membrane proteins have advanced in simulation time length, regarding ensemble channel action, and by addressing protein-protein interactions within a membrane (Chandler *et al.*, 2008, Jensen *et al.*, 2008). We suggest that large-scale simulations should be performed with respect to OM β-barrel porins, hopefully elucidating

existence of energetic minima that govern porin assembly and eventual modifications of function due to molecular crowding.

Based on the above analysis of the trimer porin order in AFM topographs and the high similarity between the porins from *Rb. capsulatus* and *R. denitrificans*, we used the *Rb. capsulatus* porin structure to build a model (Scheuring et al., 2007) of the supra-molecular assembly of porins in the native OM. This model suggests that peripheries of the porin barrels are fit into the 'grooves' between two monomers of the neighboring trimers (**Fig. 5A**).

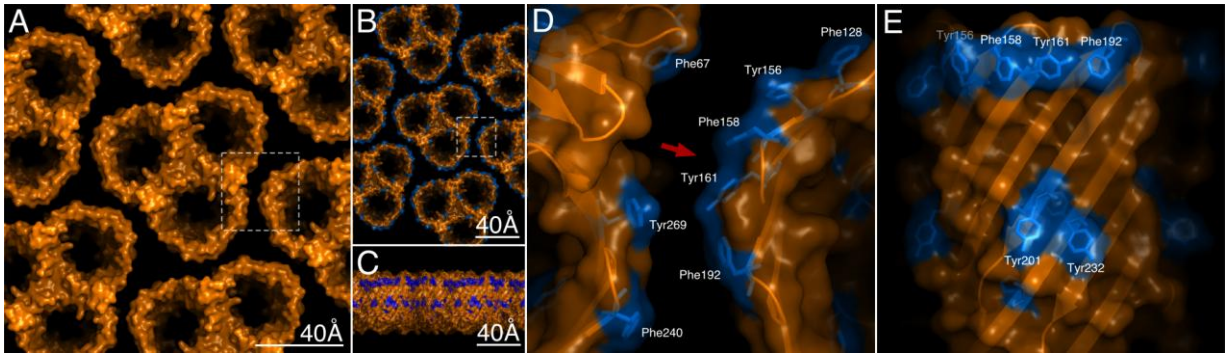

Fig. 5) Atomic model of the native supramolecular assembly of porins in the OM. **(A)** supramolecular porin assembly in the OM deduced from the high resolution AFM analysis (see figure 5). **(B)** In all so far known porin structures, the barrels have peripheral girdles of aromatic amino acid residues (blue). **(C)** View in the membrane plane with the periplasmic surface up: aromatic residues form two girdles delineating the membrane boarders. **(D)** Close-up views on the interaction region between neighboring porins (dashed outline in A and B). On the periplasmic surface, dense clusters of aromatics (Y156, F158, Y161, F192) from strands b8, b9, and b10 of one porin interact with aromatics (F240, Y269, F67) from b12 and b14 of the neighboring porin trimer. **(E)** View of the contact interface of the peripheral surface of the porin (indicated by red arrow in D): on the extracellular girdle aromatics (Y201, Y232) from strands b11 and b12 interact with (Y14, W19) from b1 and b2 of neighboring trimers.

Since the first structure resolution of an outer membrane porin, *E. coli* OmpF (Cowan et al., 1992), it has been observed that porins feature aromatic residues on the interface between the lipid bilayer and the aqueous environment (**Fig. 5B**) organized in two well-defined girdles (**Fig. 5C**). This is a general characteristic of all porins of known structure and other OM proteins (Nikaido, 2003). However, a conclusive explanation is still lacking. It has been proposed that the

aromatic residues protect the adjacent polar/non-polar surfaces of the protein at the membrane border, from unfavorable interactions, which may result from vertical protein displacement (Kreusch et al., 1994). Other studies have examined the physical basis for such a location of aromatic residues, but this on a single molecule level (Sun *et al.*, 2008, Yau *et al.*, 1998). Given our finding, that each porin in the native OM is in contact with neighboring porin molecules, we propose a novel interpretation for the preference of aromatic residues for the porin surfaces. The bulkiness of these residues makes that aromatics are exposed furthest out from the periphery of the porin barrels (**Fig. 5D**), notably at the barrel surface exposed to the neighboring trimer (**Fig. 5E**). Therefore, they might play a key role in mediating intermolecular interactions, which stabilize the supramolecular architecture of porins in the native OM.

Structure and flexibility of hairpins on the periplasmic surface

Depending on minute differences in force applied on the sample, we have been able to probe two conformations of the periplasmic turns, which were easily distinguishable in unprocessed topographs (**Fig. 6A, B**). Those results were obtained reversibly, on the same patch of the OM and over several scanning cycles. Averages (Fechner et al., 2009) revealed that under higher loading force (**Fig. 6C**, right), the apparent height of the prominent periplasmic inter-channel protrusions (β2-β3 and β14-β15) decreased compared to the low-force average (**Fig. 6C**, left). Consequently, the central indentation was less apparent and inter-subunit walls became visible, as evidenced by section analysis (**Fig. 6D**). Calculation of the standard deviation map (Scheuring *et al.*, 2002, Müller *et al.*, 1998) confirmed flexibility of the periplasmic porin turns scanned at low forces (**Fig. 6E**). The flexibility reported here by AFM, can be referred to high B-factors in the X-ray structures of the periplasmic hair-pin turns of other α-proteobacterial porins (Kreusch et al., 1994). By comparison with the structure of the *Rb. capsulatus* porin colored by B-factor (**Fig. 6F**), we confirm that the measured flexibility concerns the β2-β3 turn.

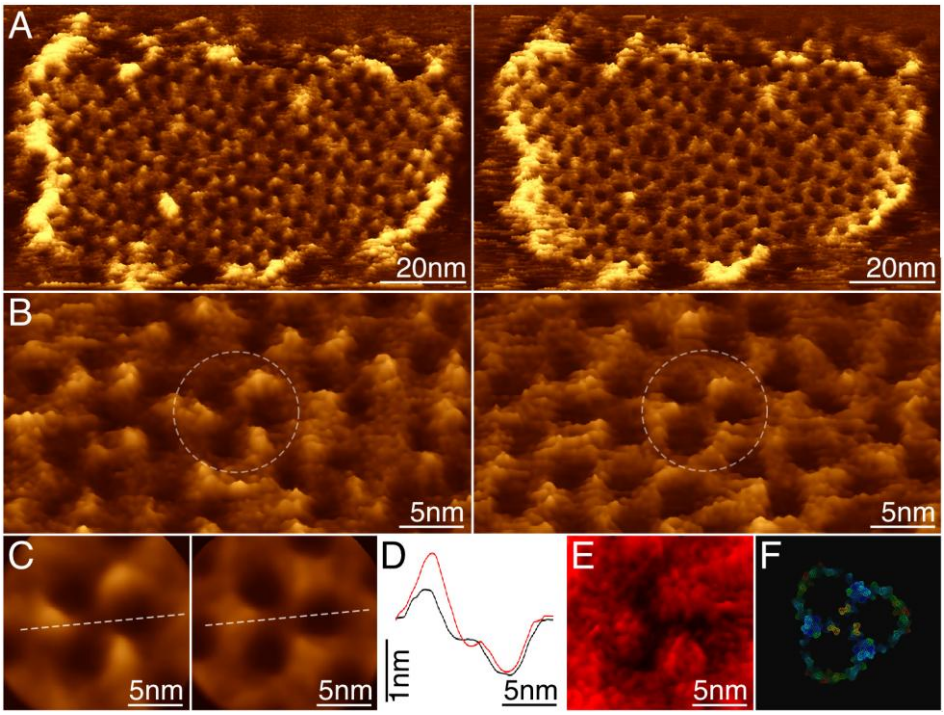

Fig. 6) Probing flexibility of the periplasmic β-strand turns of the *R. denitrificans* porin. Overview **(A)** and high-resolution **(B)** images of the same patch of the outer membrane scanned at minimal (left) and elevated (+~50pN) (right) forces. Typical trimer is encircled for clarity. **(C)** Three-fold symmetrized averages (*n=30*) highlight the changes of the peripheral inter-channel protrusion observed at low force imaging (left) and at higher forces (right). **(D)** Section analysis along the dashed lines in (C). **(E)** Standard deviation map (0.3Å ≤ SD ≤ 3.1Å) of the low-force average (C) reveals high position variability of the peripheral protrusions. **(F)** Mesh representation of the periplasmic surface of the *R. capsulatus* porin rendered in default B-factor coloring.

Analysis of amino acid sequence and surface structure of the R. denitrificans porin compared to homologous porins of known structure

In order to deduce the maximum structural information from our porin topographs, we carried out a sequence alignment (**Fig. 7A**) of the *R. denitrificans* porin with two α-proteobacterial porins of known X-ray structure from *Rb. capsulatus* (PDB: 2POR; (Weiss et al., 1991), *Rb. blasticus* (PDB: 1PRN; (Kreusch et al., 1994) and OmpF from *E. coli*, for which both the X-ray structure (PDB: 2OMF; (Cowan et al., 1992) and AFM imaging data are available (Schabert

& Engel, 1994, Müller & Engel, 1999). Although those structures show that the periplasmic surfaces of the α-proteobacterial porins are rather similar, (**Fig. 7B**, upper panel), the extracellular surfaces display high contour variability (**Fig. 7B**, bottom panel) what reflects differences on the sequence level (Welte et al., 1995).

Because alignment programs such a CLUSTALW have difficulty to differentiate between β-strands and variable loops when introducing gaps to an alignment, their results have to be manually corrected (Nikaido, 2003, Jeanteur *et al.*, 1991). Those corrections are based on identification of sequence regions, which are likely to form β-strands or loops. To achieve this task, we employed a set of prediction algorithms, previously evaluated for alignments of sequences of proteins forming transmembrane β-barrels (see Materials and methods). We obtained an alignment of the OM porin sequences from *R. denitrificans*, *Rb. capsulatus*, *Rb. blasticus* and *E. coli* and identified the landmarks of all bacterial major porins (Nikaido & Saier, 1992): 16 β-strands, eight highly conserved periplasmic hair-pin turns and eight extracellular loops, which differed significantly in length between species (**Fig. 7A**). We did not obtain any gaps in the alignment among the α-proteobacterial porins in the periplasmic turns regions (with exception of a single residue insertion at loop β10-β11 in the *Rb. blasticus* sequence). This is in accordance with previous observations that short, hair-pin connections of β-strands on the periplasmic side show little variability among bacterial porins (Welte et al., 1995). For this reason, our topographs of this side of the porin can be readily compared to X-ray structures of the abovementioned α-proteobacterial porins and particularly with the porin from *Rb. capsulatus* (**Fig. 7B**, upper panel). Based on the striking similarity between the AFM average and the X-ray structure, as well as on high conservation of amino acid sequences in the periplasmic turns regions between the two porins, we deduce that the major protrusions correspond to loop β2-β3 and β14-β15 and the small axial protrusions to the N-terminal aspartate, and a faint protrusion

emerging from turn β12-β13 (**Fig. 7A, B**, see also figure 4). On the other hand, the periplasmic side of *E. coli* OmpF displays elongated protrusions that meet at the trimer axis (**Fig. 7B**, upper panel) and which correspond to insertions of nine amino acids at the N-terminus and of six residues at turn β6-β7 (**Fig. 7A**).

Extracellular loop β11-β12, which forms a large globular domain in *Rb. capsulatus* (Kreusch & Schulz, 1994) and co-forms with neighbor extracellular loops the extracellular protrusions on the *E. coli* OmpF, is shorter by about 11 residues in the sequences of *R. denitrificans* and *Rb. blasticus.* This deletion results in a flat extracellular surface of *Rb. blasticus* porin in comparison to the *Rb. capsulatus* porin (**Fig. 7B**, bottom panel) (Kreusch et al., 1994). However, in our topographs the porin of *R. denitrificans* displays major protrusions, which we annotate to an insertion of about 11 amino acids in loop β13-β14. It also features insertions in extracellular loops β1-β2 and β3-β4, which in other porins of known structure, are located close to subunit interfaces. Similar insertions in the porin from *Rb. blasticus* increase its height at the trimer axis when compared to the *Rb. capsulatus* (Kreusch & Schulz, 1994). Moreover, the loop β3-β4, which folds into the channel's cavity and narrows its diameter, is longer in *R. denitrificans*, which may result in decreased diffusion rates of the channel. This is in remarkable agreement with a conductivity study, which revealed that the *R. denitrificans* porin had single channel conductance up to 1 nS lower than that of the related freshwater homologues from the α-proteobacteria (Neumann et al., 1997). Since this conductivity characteristic is distinctive for porins from other halophilic species (Wolf et al., 1996), this could be an evolutionary adaptation that those bacteria developed in order to deal with high salt concentration in their environment. We therefore propose that the extracellular side of the native porin from *R. denitrificans* resembles that of *Rb. blasticus* with respect to the interface height and to the *Rb. capsulatus* porin as far as the large protruding loops are concerned (**Fig. 7B**).

This is the first time the entire amino acid sequence of the *R. denitrificans* porin has been analyzed and its implications to the tertiary structure of the native protein have been proposed.

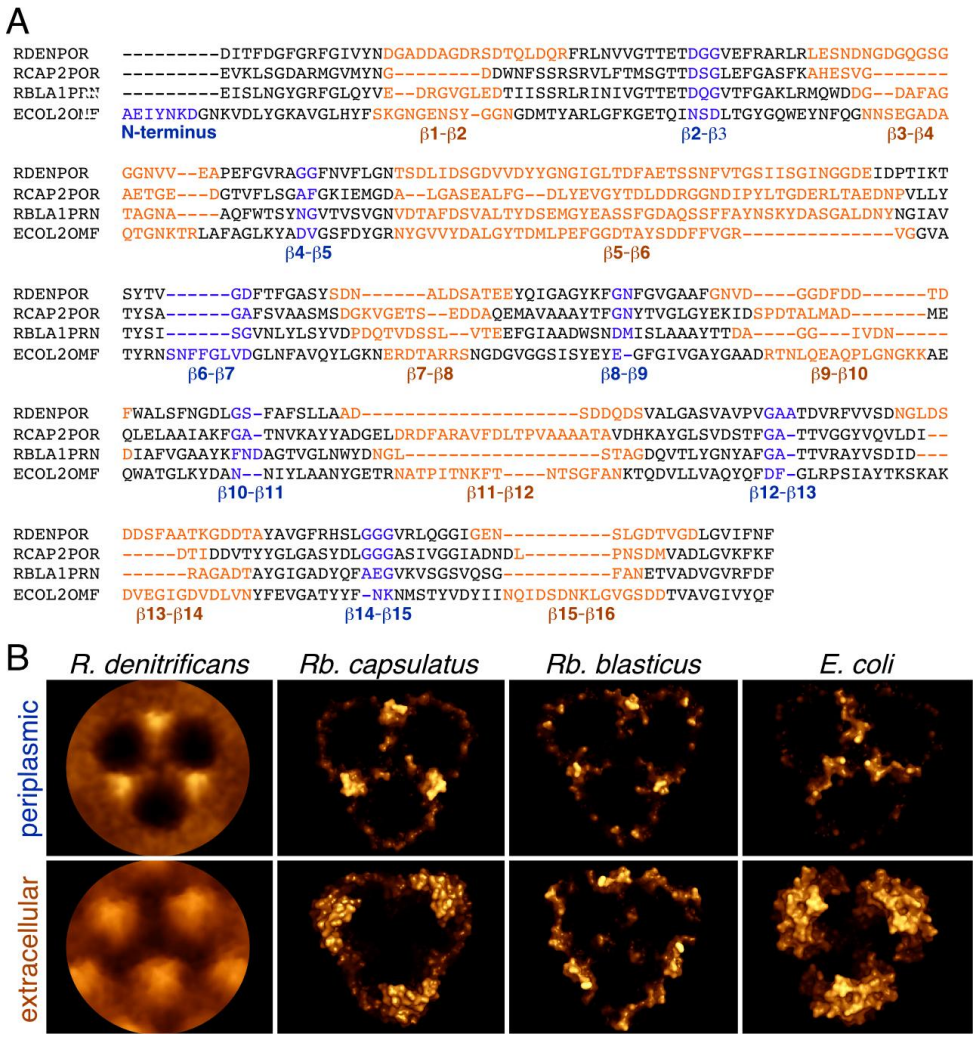

Fig. 7) Detailed sequence and structure comparison between the *R denitrificans* porin and homologous porins of known structure. (A) Sequence alignment of OM porins from *R. denitrificans* (RDENPOR), *Rb. capsulatus* (RCAP1PRN), *Rb. blasticus* (RBLA2POR) and OmpF porin from *E. coli* (ECOL2OMF). 16 transmembrane β-strands are marked in black, periplasmic turns in blue and extracellular loops in orange. The alignment of (RBLA2POR), (RCAP1PRN) and (ECOL2OMF) is that of Nikaido (Nikaido, 2003) with minor modifications. The sequence of RDPOR was aligned as described in materials and methods. **(B)** Comparison of the AFM topographies of the periplasmic side (upper panel) and the extracellular side (lower panel) of the *R. denitrificans* porin with X-ray structures of other porins: *Rb. blasticus* (PDB: 2POR), *Rb. capsulatus* (PDB: 1PRN) and OmpF porin from *E. coli* (PDB: 2OMF).

Experimental procedures

Preparation of the outer membrane

The washed bacteria were re-suspended in 20mM Tris-HCl pH7.5 buffer to a final concentration of 400 UOD/ml. Cell concentration was measured in OD units at 600 nm. Lysozyme was added to a final concentration of 1.6 mg/ml, DNAse to a final concentration of 100 μg/mL, RNAse to a final concentration of 20 μg/ml and anti-protease cocktail according to the manufacturers instructions (Roche). Cells were broken by two passages through the French Pressure cell at 1200 psi (8300 kPa). Unbroken cells were removed by centrifuging at 10,000 *g* for 15 min. The large outer membrane fragments were collected by ultra-centrifugation (40,000 rpm for 5 min in a Ti70 rotor). The pellet was re-suspended in a 20mM Tris-HCl pH7.5 buffer with anti-protease cocktail and 20% sucrose. This sample was loaded onto a discontinuous sucrose gradient containing 2 ml of 70% sucrose, 7 ml of 50% sucrose and centrifuged 16 hours (overnight) at 39,000 rpm in a SW40 swinging bucket rotor (192,000 *g*). The purified OM fraction was collected from the interface between the 70% sucrose and 50% sucrose.

Sequence alignment

The translated sequence of the gene RD1_0047 (Swingley et al., 2007) was used as the amino acid sequence of the *R. denitrificans* porin (gi|110677464) and sequences gi|443427, gi|640363 , and gi|1310953 of *Rb. capsulatus*, *Rb. blasticus* and *E. coli* porins respectively. An initial CLUSTALW alignment of the sequences showed that the first 20 amino acids of the gi|110677464 were absent in the mature, homologue proteobacterial proteins and were trimmed for further alignments. The alignment of the *Rb. capsulatus*, *Rb. blasticus* and *E. coli* porin sequences is that of Nikaido (Jeanteur et al., 1991, Nikaido, 2003) with minor modifications. The sequence of *R. denitrificans* porin was added on the basis of predictions of the most recent

Hidden Markov Model method, which was validated for the transmembrane strands and the topology of beta-barrel outer membrane proteins of Gram-negative bacteria (PRED-TMBB, http://bioinformatics.biol.uoa.gr/PRED-TMBB) (Bagos et al., 2004). The approximate locations of β-strands and turns were confirmed by the Jeanteur method (Jeanteur et al., 1991, Nikaido, 2003): we used the plot of (average hydrophobicity plus hydrophobic moment) to identify β-strands and the Paul and Rosenbusch criteria to predict the loops (Paul & Rosenbusch, 1985). Additionally, we crosschecked the sequence interpretations with the known X-ray structures.

Genome analysis

The complete genome of *R. denitrificans* OCh 114 (GenBank: CP000362) was analyzed with on-line tools accessible through the (http://www.ncbi.nlm.nih.gov) website. Outer membrane proteins were indentified among the 3946 protein-coding genes by their description and homology to known 3-D structures retrieved by the MMDB module (Wang et al., 2007). The total number of genes coding for outer membrane proteins in the *R. denitrificans* genome was assessed by the BOMP platform (Berven et al., 2004) and compared to data that was previously published by the authors that analyzed the *E. coli* genome.

Atomic force microscopy (AFM)

The AFM was operated in contact mode at ambient temperature and pressure in buffer solution. Imaging was performed with a commercial Nanoscope-E AFM (Veeco, Santa Barbara, CA, USA) equipped with a 160-µm scanner (J-scanner) and oxide-sharpened Si_3N_4 cantilevers (length 100 µm; k = 0.09 N/m; Olympus Ltd., Tokyo, Japan). For imaging, minimal loading forces of ~100 pN were applied at scan frequencies of 4-7 Hz using optimized feedback parameters. Mica supports were immerged in 20 µl adsorption buffer: 10 mM Tris-HCl, pH 7.2,

25 mM MgCl. Subsequently, 1 µl of the outer membrane isolate was injected into this buffer. After 15min of adsorption to the mica support, the sample was rinsed with the recording buffer (10mM Tris-HCl, pH 7.2, 150mM KCl) and imaging was performed.

Image analysis and structural models:

Image analysis, averaging and standard deviation map calculation was performed using cross-correlation based in-house routines for the ImageJ image processing package (Scheuring et al., 2007, Fechner et al., 2009). X-ray structures of OM porins from *Rb. blasticus* (PDB: 2POR), *Rb. capsulatus* (PDB: 1PRN) and *E. coli* (PDB: 2OMF) were rendered in molecular surface or mesh representation with PyMol (DeLano, 2002) and colored by the z atomic coordinates (normal to the membrane plane) for easier comparison with the AFM topographs.

Acknowledgements:

This study was supported by a ANR PNANO-06-023 grant (to S.S and J.S) and by a research support grant by the 'Ville de Paris' (to S.S).

References:

Bagos, P. G., T. D. Liakopoulos, I. C. Spyropoulos & S. J. Hamodrakas, (2004) PRED-TMBB: a web server for predicting the topology of beta-barrel outer membrane proteins. *Nucleic Acids Res* **32**: W400-404.

Berven, F. S., K. Flikka, H. B. Jensen & I. Eidhammer, (2004) BOMP: a program to predict integral beta-barrel outer membrane proteins encoded within genomes of Gram-negative bacteria. *Nucleic Acids Res* **32**: W394-399.

Binnig, G., C. F. Quate & C. Gerber, (1986) Atomic force microscope. *Phys. Rev. Lett.* **56**: 930-933.

Bond, P. J. & M. S. Sansom, (2004) The simulation approach to bacterial outer membrane proteins. *Mol Membr Biol* **21**: 151-161.

Buehler, L. K., S. Kusumoto, H. Zhang & J. P. Rosenbusch, (1991) Plasticity of *Escherichia coli* porin channels. *J. Biochem. Chem.* **266**: 24446-24450.

Buzhynskyy, N., R. K. Hite, T. Walz & S. Scheuring, (2007) The supramolecular architecture of junctional microdomains in native lens membranes. *EMBO Reports* **8**: 51-55.

Chandler, D. E., J. Hsin, C. B. Harrison, J. Gumbart & K. Schulten, (2008) Intrinsic curvature properties of photosynthetic proteins in chromatophores. *Biophysical Journal* **95**: 2822-2836.

Cowan, S. W., T. Schirmer, G. Rummel, M. Steiert, R. Ghosh, R. A. Pauptit, J. N. Jansonius & J. P. Rosenbusch, (1992) Crystal structures explain functional properties of two *E. coli* porins. *Nature* **358**: 727-733.

DeLano, W. L., (2002) The PyMOL Molecular Graphics System, http://www.pymol.org.

Domene, C., P. J. Bond & M. S. Sansom, (2003) Membrane protein simulations: ion channels and bacterial outer membrane proteins. *Adv Protein Chem* **66**: 159-193.

Dufrêne, Y., (2008) Towards nanomicrobiology using atomic force microscopy. *Nat Rev Microbiol* **6**: 674-680.

Engelman, D., (2005) Membranes are more mosaic than fluid. *Nature* **438**: 578-580.

Fechner, P., T. Boudier, S. Mangenot, S. Jaroslawski, J. N. Sturgis & S. Scheuring, (2009) Resolution, noise and structural information in high-resolution AFM topographs. *Biophys J* **96**: 3822-3831.

Gatsos, X., A. J. Perry, K. Anwari, P. Dolezal, P. P. Wolynec, V. A. Likic, A. W. Purcell, S. K. Buchanan & T. Lithgow, (2008) Protein secretion and outer membrane assembly in Alphaproteobacteria. *FEMS Microbiol Rev* **32**: 995-1009.

Hoenger, A., J. M. Pages, D. Fourel & A. Engel, (1993) The orientation of porin OmpF in the outer membrane of Escherichia coli. *J Mol Biol* **233**: 400-413.

Jeanteur, D., J. H. Lakey & F. Pattus, (1991) The bacterial porin superfamily: sequence alignment and structure prediction. *Mol Microbiol* **5**: 2153-2164.

Jensen, M. O., R. O. Dror, H. F. Xu, D. W. Borhani, I. T. Arkin, M. P. Eastwood & D. E. Shaw, (2008) Dynamic control of slow water transport by aquaporin 0: Implications for hydration and junction stability in the eye lens. *Proceedings of the National Academy of Sciences of the United States of America* **105**: 14430-14435.

Karrasch, S., R. Hegerl, J. Hoh, W. Baumeister & A. Engel, (1994) Atomic force microscopy produces faithful high-resolution images of protein surfaces in an aqueous environment. *Proc. Natl. Acad. Sci. U.S.A.* **91**: 836-838.

Khalid, S., P. J. Bond, S. S. Deol & M. S. Sansom, (2006) Modeling and simulations of a bacterial outer membrane protein: OprF from Pseudomonas aeruginosa. *Proteins* **63**: 6-15.

Kreusch, A., A. Neubuser, E. Schiltz, J. Weckesser & G. Schulz, (1994) Structure of the membrane channel porin from Rhodopseudomonasblastica at 2.0 Å resolution. *Protein Sci* **3**: 58-63.

Kreusch, A. & G. Schulz, (1994) Refined structure of the porin from Rhodopseudomonas blastica. Comparison with the porin from Rhodobacter capsulatus. *Journal of Molecular Biology* **243**: 891-905.

Lambert, O., G. S. Moeck, D. Lévy, L. Plancon, L. Letellier & R. JL., (1999) An 8-A projected structure of FhuA, A "ligand-gated" channel of the Escherichia coli outer membrane. *J Struct Biol.* **15**: 2.

Locher, K. P., A. T. Lee & D. C. Rees, (2002) The E. coli BtuCD structure: a framework for ABC transporter architecture and mechanism. *Science* **296**: 1038-1040.

Müller, D. J. & A. Engel, (1999) Voltage and pH induced channel closure of porin OmpF visualised by atomic force microscopy. *J. Mol. Biol.* **285**: 1347-1351.

Müller, D. J., D. Fotiadis & A. Engel, (1998) Mapping flexible protein domains at subnanometer resolution with the AFM. *FEBS Lett.* **430**: 105-111.

Müller, D. J., D. Fotiadis, S. Scheuring, C. Moeller & A. Engel, (2000) Conformational changes, flexibilities and intramolecular forces observed on individual proteins using AFM. *Single Molecules* **1**: 115-118.

Neumann, U., E. Maier, E. Schiltz, J. Weckesser & R. Benz, (1997) Characterization of porin from Roseobacter denitrificans. *Antonie Van Leeuwenhoek* **72**: 135-140.

Nikaido, H., (2003) Molecular basis of bacterial outer membrane permeability revisited
. *Microbiol Mol Biol Rev* **67**: 593-656.

Nikaido, H. & M. H. Saier, (1992) Transport proteins in bacteria: common themes in their design. *Science* **258**: 936-942.

Paul, C. & J. P. Rosenbusch, (1985) Folding patterns of porin and bacteriorhodopsin. *EMBO J* **4**: 1593-1597.

Pautsch, A. & G. Schulz, (2000) High-resolution structure of the OmpA membrane domain. *J Mol Biol* **298**: 273-282.

Rosenbusch, P., (1974) Characterization of the major envelope protein from *Escherichia coli*. *J. Biol. Chem.* **249**: 8019-8029.

Schabert, F. A. & A. Engel, (1994) Reproducible acquisition of *Escherichia coli* porin surface topographs by atomic force microscopy. *Biophys. J.* **67**: 2394-2403.

Schabert, F. A., C. Henn & A. Engel, (1995) Native *Escherichia coli* OmpF porin surfaces probed by atomic force microscopy. *Science* **268**: 92-94.

Scheuring, S., T. Boudier & J. N. Sturgis, (2007) From high-resolution AFM topographs to atomic models of supramolecular assemblies. *J Struct Biol* **159**: 268-276.

Scheuring, S., J. Busselez & D. Levy, (2005) Structure of the dimeric PufX–containing core complex of Rhodobacter blasticus by in situ AFM. *J. Biol. Chem.* **180**: 1426-1431.

Scheuring, S., D. J. Müller, H. Stahlberg, H.-A. Engel & A. Engel, (2002) Sampling the conformational space of membrane protein surfaces with the AFM. *Eur. Biophys. J.* **31**: 172-178.

Scheuring, S., P. Ringler, M. Borgina, H. Stahlberg, D. J. Müller, P. Agre & A. Engel, (1999) High resolution topographs of the *Escherichia coli* waterchannel aquaporin Z. *EMBO J.* **18**: 4981-4987.

Scheuring, S., J. Seguin, S. Marco, D. Lévy, B. Robert & J. L. Rigaud, (2003) Nanodissection and high-resolution imaging of the *Rhodopseudomonas viridis* photosynthetic core-complex in native membranes by AFM. *Proc. Natl. Acad. Sci. U.S.A.* **100**: 1690-1693.

Scheuring, S., J. N. Sturgis, V. Prima, A. Bernadac, D. Lévy & J.-L. Rigaud, (2004) Watching the photosynthetic apparatus in native membranes. *Proc. Natl. Acad. Sci. U.S.A.* **101**: 11293-11297.

Schirmer, T., (1998) General and specific porins from bacterial outer membranes. *J. Stuct. Biol.* **121**: 101-109.

Seelert, H., A. Poetsch, N. A. Dencher, A. Engel, H. Stahlberg & D. J. Müller, (2000) Proton powered turbine of a plant motor. *Nature* **405**: 418-419.

Shultis, D., M. Purdy, C. Banchs & M. Wiener, (2006) Outer membrane active transport: structure of the BtuB:TonB complex. *Science* **312**: 1396-1399.

Singer, S. J. & G. L. Nicolson, (1972) The fluid mosaic model of the structure of cell membranes. *Science* **175**: 720-731.

Sun, H., D. V. Greathouse, O. S. Andersen & R. E. Koeppe, 2nd, (2008) The preference of tryptophan for membrane interfaces: insights from N-methylation of tryptophans in gramicidin channels. *J Biol Chem* **283**: 22233-22243.

Swingley, W. D., S. Sadekar, S. D. Mastrian, H. J. Matthies, J. Hao, H. Ramos, C. R. Acharya, A. L. Conrad, H. L. Taylor, L. C. Dejesa, M. K. Shah, E. O'Huallachain M, M. T. Lince, R. E. Blankenship, J. T. Beatty & J. W. Touchman, (2007) The complete genome sequence of Roseobacter denitrificans reveals a mixotrophic rather than photosynthetic metabolism. *J Bacteriol* **189**: 683-690.

Todt, J. C., W. J. Rocque & E. J. McGroarty, (1992) Effects of pH on bacterial porin function. *Biochem.* **31**: 10471-10478.

Vogt, J. & G. Schulz, (1999) The structure of the outer membrane protein OmpX from Escherichia coli reveals possible mechanisms of virulence. *Structure* **7**: 1301-1309.

Wang, Y., K. Addess, J. Chen, L. Geer, J. He, S. He, S. Lu, T. Madej, A. Marchler-Bauer, P. Thiessen, N. Zhang & S. Bryant, (2007) MMDB: annotating protein sequences with Entrez's 3D-structure database. *Nucleic Acids Res* **35**: 298-300.

Weiss, M. & G. Schulz, (1992) Structure of porin refined at 1.8 A resolution. *J Mol Biol. 1992 Sep 20;227(2):493-509.*

Weiss, M. S., A. Kreusch, E. Schlitz , U. Nestel, W. Welte, J. Weckesstr & G. E. Schulz, (1991) The structure of perth from Rhodobacter capsulatus at

1.8 A resolution *FEBS* **280**: 379-382.

Welte, W., U. Nestel, T. Wacker & K. Diederichs, (1995) Structure and function of the porin channel. *Kidney Int* **48**: 930-940.

Wolf, E., M. Zahr, R. Benz, J. F. Imhoff, A. Lustig, E. Schiltz, J. Stahl-Zeng & J. Weckesser, (1996) The porins from the halophilic species Ectothiorhodospira shaposhnikovii and Ectothiorhodospira vacuolata. *Arch Microbiol* **166**: 169-175.

Yau, W. M., W. C. Wimley, K. Gawrisch & S. H. White, (1998) The preference of tryptophan for membrane interfaces. *Biochemistry-Us* **37**: 14713-14718.